Supporting Information for:

The Open, the Closed, and the Empty: Time-resolved Fluorescence Spectroscopy and Computational Analysis of RC-LH1 Complexes from *Rhodopseudomonas palustris*

Sebastian R. Beyer[1+], Lars Müller[2+], June Southall[3], Richard J. Cogdell[3], G. Matthias Ullmann[2]*, Jürgen Köhler[1]*

[1]) Experimental Physics IV and BIMF, University of Bayreuth, 95440 Bayreuth, Germany

[2]) Computational Biochemistry/Bioinformatics, University of Bayreuth, 95440 Bayreuth, Germany

[3]) Institute of Molecular, Cell and Systems Biology, College of Medical Veterinary and Life Sciences, Biomedical Research Building, University of Glasgow, Glasgow G12 8QQ, Scotland, U.K.

[+]) These authors contributed equally to this work

*) To whom correspondence should be addressed: juergen.koehler@uni-bayreuth.de, matthias.ullmann@uni-bayreuth.de

Table of Contents

1. Number of Pulses that Consecutively Excite the Sample

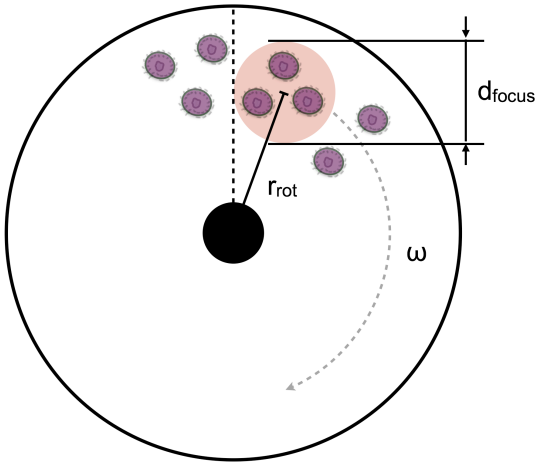

Figure S1 *Schematic representation of the spatial position of the laser focus (red shaded area) with respect to the cuvette that rotates at an angular velocity ω. The distance between the laser focus and the rotation axis is denoted as r_{rot}, and the diameter of the laser focus is given as d_{focus}. The purple ellipses symbolize RC-LH1 complexes in solution (not to scale).*

During the rotation of the cuvette, a volume element that contains the solution of RC-LH1 complexes and which passes through the laser focus is exposed to several consecutive laser pulses N_{pulse}. The average number of which can be obtained from

$$N_{pulse} = \frac{d_{focus}}{r_{rot} \cdot \sin\left(\frac{\omega}{\nu_{rep}}\right)} \qquad \text{(eq. S1)}$$

where d_{focus} = 73.6 µm denotes the diameter of the laser focus, r_{rot} = 9.5 mm corresponds to the distance of the laser focus from the rotation axis, see fig.S1, $\omega = 360° \cdot 48\ s^{-1}$ is the angular velocity, and ν_{rep} refers to the repetition rate of the laser. This yields N_{pulse} = 2, 21, 208, 2080 for repetition rates of 81 kHz, 810 kHz, 8.1 MHz, 81 MHz, respectively.

2. Convergence of the Simulations

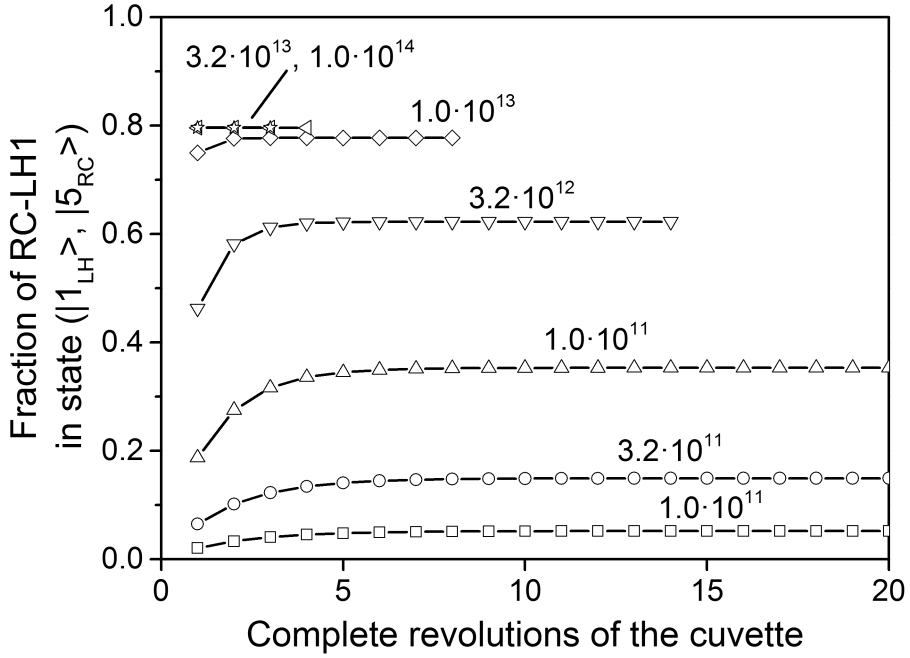

Figure S2 *Relative fraction of RC-LH1 complexes in the microstate* $\left(|1_{LH}\rangle, |5_{RC}\rangle\right)$ *as a function of the number of complete revolutions of the rotating cuvette, obtained from the simulations. The repetition rate for the excitation was 810 kHz, the photon fluence is given within the graph in units of photons/(pulse·cm²). The relative fraction of RC-LH1 complexes in microstate* $\left(|1_{LH}\rangle, |5_{RC}\rangle\right)$ *serves as an indicator for the convergence of the simulated system.*

Initially the relative fraction of RC-LH1 complexes in microstate $\left(|1_{LH}\rangle, |5_{RC}\rangle\right)$ rises as a function of the number of revolutions and then levels off. For the two highest fluences this plateau is already reached after the first revolution of the cuvette. Fluorescence transients were simulated after the population of microstate $\left(|1_{LH}\rangle, |5_{RC}\rangle\right)$ had converged.

3. Simulated Fluorescence Transients in Absence and Presence of Q_B

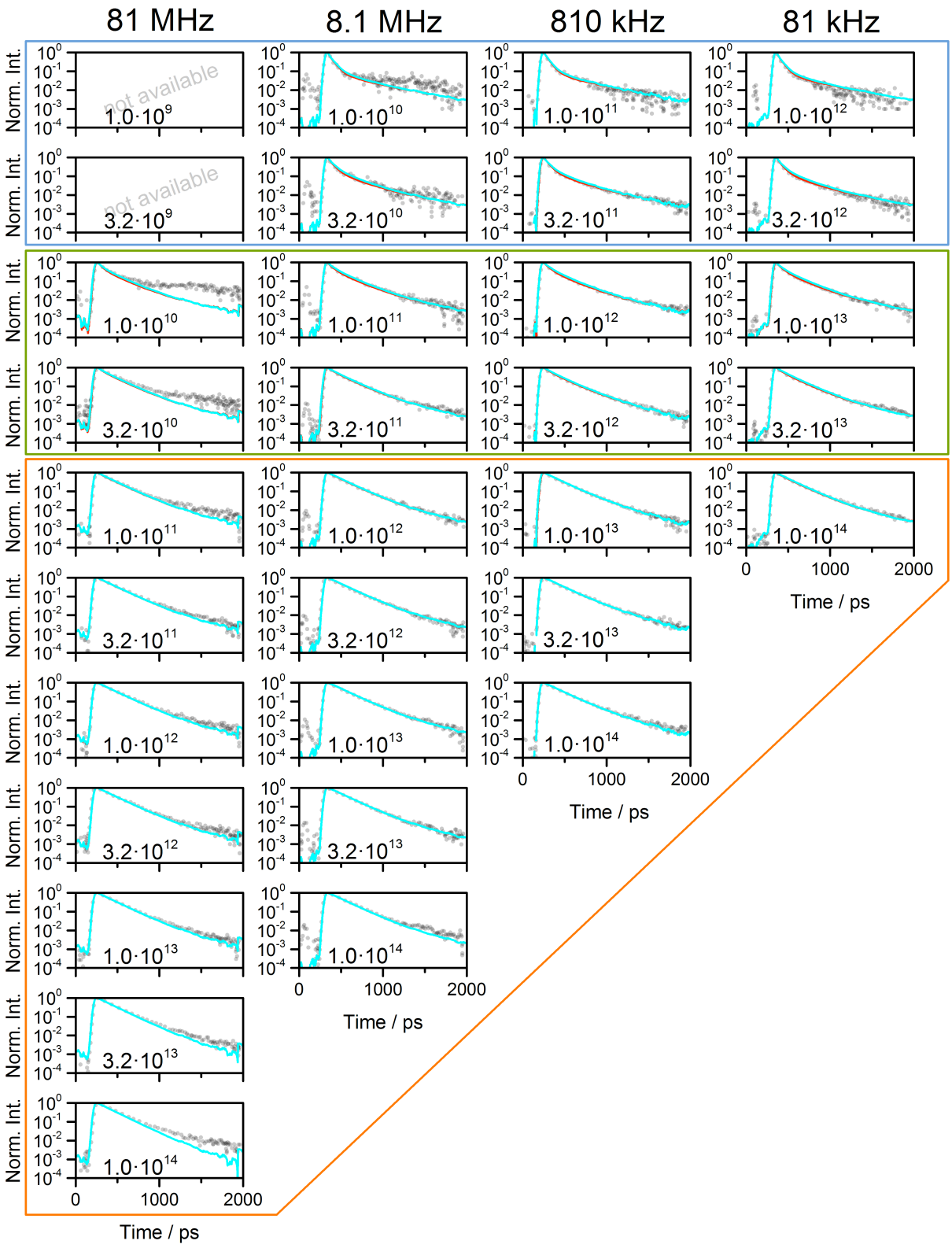

Figure S3 *Normalised fluorescence decays (black dots) of isolated RC-LH1 complexes in detergent solution as a function of the repetition rate (columns) and the photon fluence (rows)*

of the excitation together with simulated fluorescence decays (red and blue lines). The blue lines refer to simulations in the presence of Q_B using $k'_{51} = (1\ s)^{-1}$. For comparison, the red lines correspond to the simulations as provided in the main manuscript, and which were conducted under the assumption, that Q_B is not present in the samples using $k'_{51} = (100\ ms)^{-1}$. The red lines are barely visible and are almost fully masked by the blue ones. The coloured boxes indicate the range of excitation parameters for which we find from the simulations that the majority of RC-LH1 complexes is in an open state (more than 81 % open RCs, blue box), where RCs in the open and closed state coexist (20-80 % open RCs, green box) and where RCs in the closed state dominate (below 20 % open RCs, orange box).

4. Variation of the Fraction of RC-less LH1

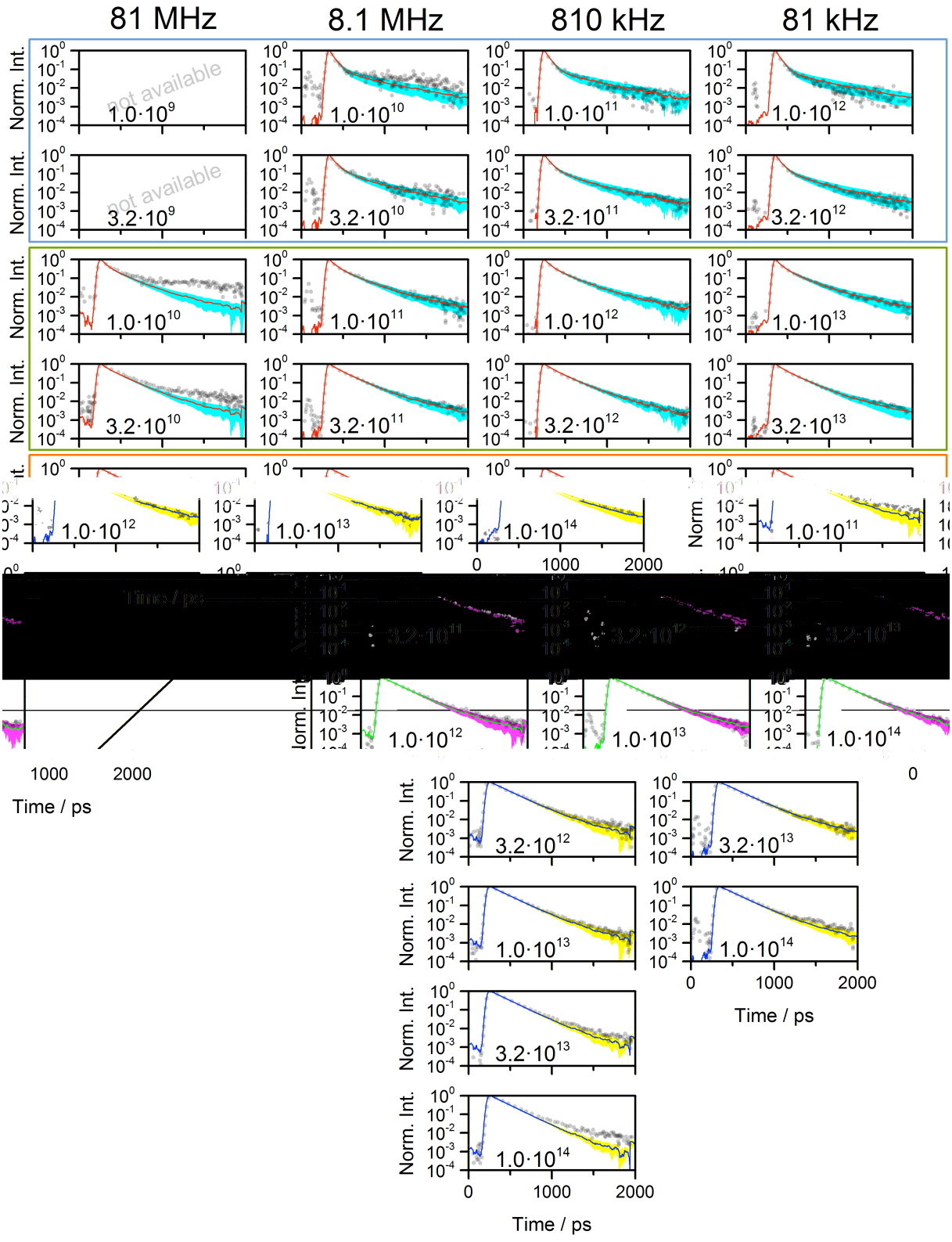

Figure S4 *Normalised fluorescence decays (black dots) of isolated RC-LH1 complexes in detergent solution as a function of the repetition rate (columns) and the photon fluence (rows)*

of the excitation together with simulated fluorescence decays (red lines and blue hose). The red lines correspond to simulated decays for a fraction of 3 % of LH1 rings without RC as provided in the main text. The blue hose gives the outer limits for varying this parameter between 1% and 5%, respectively. The coloured boxes indicate the range of excitation parameters for which we find from the simulations that the majority of RC-LH1 complexes is in an open state (more than 81 % open RCs, blue box), where RCs in the open and closed state coexist (20-80 % open RCs, green box) and where RCs in the closed state dominate (below 20 % open RCs, orange box).

5. Variation of the Fraction of Fresh RC-LH1 after Cuvette Revolution

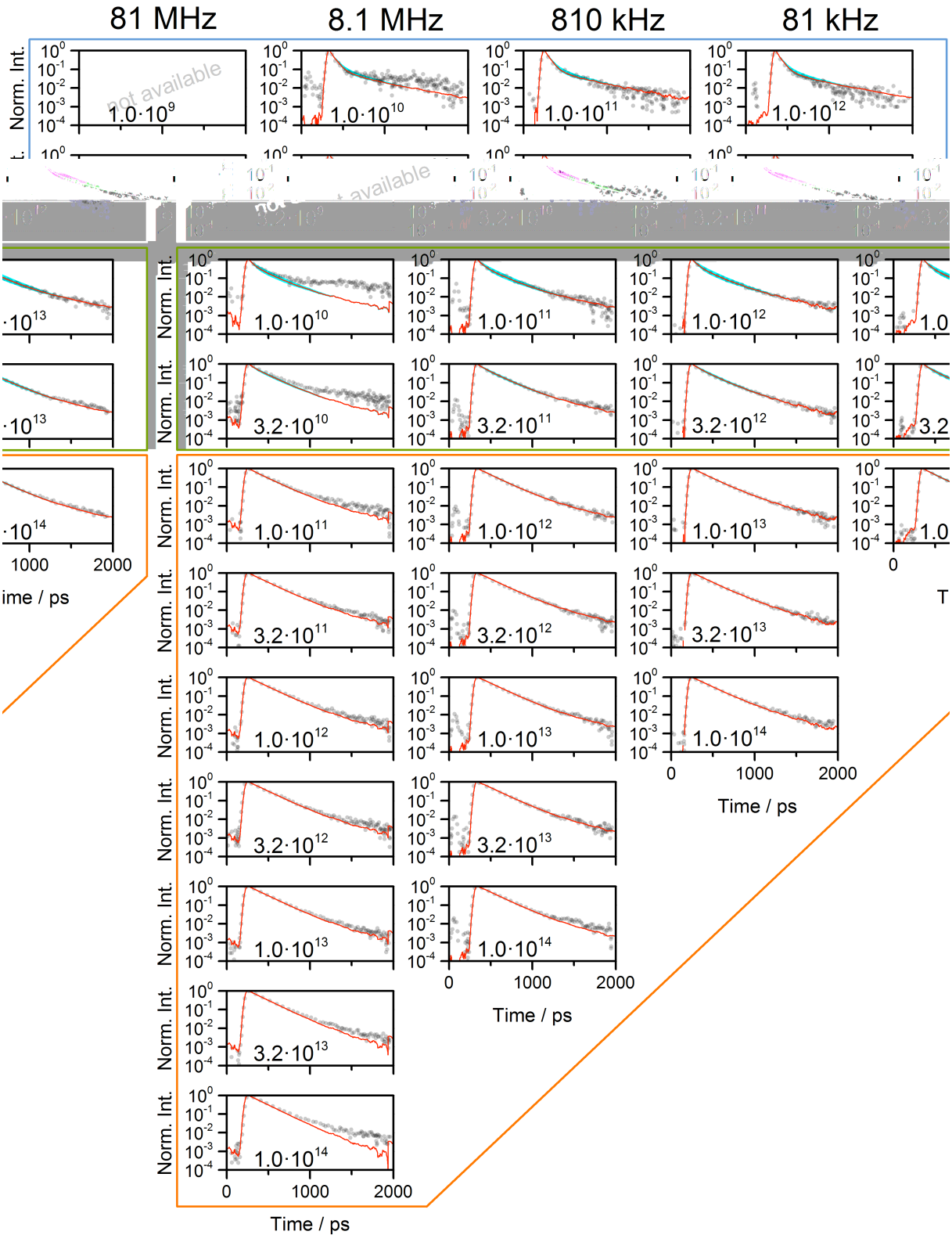

Figure S5 *Normalised fluorescence decays (black dots) of isolated RC-LH1 complexes in detergent solution as a function of the repetition rate (columns) and the photon fluence (rows)*

of the excitation together with simulated fluorescence decays (red lines and blue hose). The red lines correspond to simulated decays for a fraction of 25 % of fresh RC-LH1 complexes that enter the laser spot after one revolution of the rotating cuvette, as provided in the main text. The blue hose gives the outer limits for varying this parameter between 0 and 50%, respectively. The coloured boxes indicate the range of excitation parameters for which we find from the simulations that the majority of RC-LH1 complexes is in an open state (more than 81 % open RCs, blue box), where RCs in the open and closed state coexist (20-80 % open RCs, green box) and where RCs in the closed state dominate (below 20 % open RCs, orange box).

6. Numerical Input for figs.7A and 8B

Table S1 *Data shown in figs.7B and 8B. The relative fraction of RC-LH1 complexes that carry one or more triplet excitations is given in blue and the fraction of RC-LH1 complexes with an oxidised special pair (P^+) is given in red.*

equivalent cw excitation intensity. [photons/(s·cm²)]	repetition rate			
	81 MHz	8.1 MHz	810 kHz	81 kHz
$8.1 \cdot 10^{16}$	--	$7.0 \cdot 10^{-6}$ 0.06	$5.0 \cdot 10^{-6}$ 0.06	0.0 0.06
$2.6 \cdot 10^{17}$	--	$2.6 \cdot 10^{-5}$ 0.18	$1.8 \cdot 10^{-5}$ 0.18	0.0 0.17
$8.1 \cdot 10^{17}$	$1.2 \cdot 10^{-4}$ 0.42	$1.1 \cdot 10^{-4}$ 0.42	$7.8 \cdot 10^{-5}$ 0.42	0.0 0.42
$2.6 \cdot 10^{18}$	$5.1 \cdot 10^{-4}$ 0.74	$5.0 \cdot 10^{-4}$ 0.74	$3.5 \cdot 10^{-4}$ 0.75	0.0 0.79
$8.1 \cdot 10^{18}$	$1.9 \cdot 10^{-3}$ 0.94	$1.8 \cdot 10^{-3}$ 0.94	$1.3 \cdot 10^{-3}$ 0.95	0.0 0.96
$2.6 \cdot 10^{19}$	$6.2 \cdot 10^{-3}$ 0.97	$6.0 \cdot 10^{-3}$ 0.97	$4.1 \cdot 10^{-3}$ 0.97	
$8.1 \cdot 10^{19}$	$1.9 \cdot 10^{-2}$ 0.97	$1.9 \cdot 10^{-2}$ 0.97	$9.1 \cdot 10^{-3}$ 0.97	
$2.6 \cdot 10^{20}$	$6.0 \cdot 10^{-2}$ 0.97	$5.8 \cdot 10^{-2}$ 0.97		
$8.1 \cdot 10^{20}$	$1.7 \cdot 10^{-1}$ 0.97	$1.2 \cdot 10^{-1}$ 0.97		
$2.6 \cdot 10^{21}$	$4.4 \cdot 10^{-1}$ 0.97			
$8.1 \cdot 10^{21}$	$6.8 \cdot 10^{-1}$ 0.97			

7. Conversions to CW Excitation Intensity

Table S2 *Conversion of the photon fluence at a given repetition rate into equivalent cw excitation intensity at λ = 879 nm. Equivalent cw excitation intensities are given in dimensions of photons/(s·cm²), as used in the main text, as well as in the more common representations of W/cm² and Einsteins.*

fluence [photons/ (pulse·cm²)]	equivalent cw excitation intensity											
	[photons/(s·cm²)]				[W/cm²] (at λ = 879 nm)				[photons/(mol·s·cm²)] (Einstein)			
	81 MHz	8.1MHz	810 kHz	81 kHz	81 MHz	8.1MHz	810 kHz	81 kHz	81 MHz	8.1MHz	810 kHz	81 kHz
$1.0\cdot10^{14}$	$8.1\cdot10^{21}$	$8.1\cdot10^{20}$	$8.1\cdot10^{19}$	$8.1\cdot10^{18}$	$1.8\cdot10^{3}$	$1.8\cdot10^{2}$	$1.8\cdot10^{1}$	$1.8\cdot10^{0}$	$1.4\cdot10^{-2}$	$1.4\cdot10^{-3}$	$1.4\cdot10^{-4}$	$1.4\cdot10^{-5}$
$3.2\cdot10^{13}$	$2.6\cdot10^{21}$	$2.6\cdot10^{20}$	$2.6\cdot10^{19}$	$2.6\cdot10^{18}$	$5.9\cdot10^{2}$	$5.9\cdot10^{1}$	$5.9\cdot10^{0}$	$5.9\cdot10^{-1}$	$4.3\cdot10^{-3}$	$4.3\cdot10^{-4}$	$4.3\cdot10^{-5}$	$4.3\cdot10^{-6}$
$1.0\cdot10^{13}$	$8.1\cdot10^{20}$	$8.1\cdot10^{19}$	$8.1\cdot10^{18}$	$8.1\cdot10^{17}$	$1.8\cdot10^{2}$	$1.8\cdot10^{1}$	$1.8\cdot10^{0}$	$1.8\cdot10^{-1}$	$1.4\cdot10^{-3}$	$1.4\cdot10^{-4}$	$1.4\cdot10^{-5}$	$1.4\cdot10^{-6}$
$3.2\cdot10^{12}$	$2.6\cdot10^{20}$	$2.6\cdot10^{19}$	$2.6\cdot10^{18}$	$2.6\cdot10^{17}$	$5.9\cdot10^{1}$	$5.9\cdot10^{0}$	$5.9\cdot10^{-1}$	$5.9\cdot10^{-2}$	$4.3\cdot10^{-4}$	$4.3\cdot10^{-5}$	$4.3\cdot10^{-6}$	$4.3\cdot10^{-7}$
$1.0\cdot10^{12}$	$8.1\cdot10^{19}$	$8.1\cdot10^{18}$	$8.1\cdot10^{17}$	$8.1\cdot10^{16}$	$1.8\cdot10^{1}$	$1.8\cdot10^{0}$	$1.8\cdot10^{-1}$	$1.8\cdot10^{-2}$	$1.4\cdot10^{-4}$	$1.4\cdot10^{-5}$	$1.4\cdot10^{-6}$	$1.4\cdot10^{-7}$
$3.2\cdot10^{11}$	$2.6\cdot10^{19}$	$2.6\cdot10^{18}$	$2.6\cdot10^{17}$	--	$5.9\cdot10^{0}$	$5.9\cdot10^{-1}$	$5.9\cdot10^{-2}$	--	$4.3\cdot10^{-5}$	$4.3\cdot10^{-6}$	$4.3\cdot10^{-7}$	--
$1.0\cdot10^{11}$	$8.1\cdot10^{18}$	$8.1\cdot10^{17}$	$8.1\cdot10^{16}$	--	$1.8\cdot10^{0}$	$1.8\cdot10^{-1}$	$1.8\cdot10^{-2}$	--	$1.4\cdot10^{-5}$	$1.4\cdot10^{-6}$	$1.4\cdot10^{-7}$	--
$3.2\cdot10^{10}$	$2.6\cdot10^{18}$	$2.6\cdot10^{17}$	--	--	$5.9\cdot10^{-1}$	$5.9\cdot10^{-2}$	--	--	$4.3\cdot10^{-6}$	$4.3\cdot10^{-7}$	--	--
$1.0\cdot10^{10}$	$8.1\cdot10^{17}$	$8.1\cdot10^{16}$	--	--	$1.8\cdot10^{-1}$	$1.8\cdot10^{-2}$	--	--	$1.4\cdot10^{-6}$	$1.4\cdot10^{-7}$	--	--